Available online at www.sciencedirect.com
SCIENCE DIRECT®
Journal of Nuclear Materials 329–333 (2004) 103–111
journal of nuclear materials
www.elsevier.com/locate/jnucmat

# Multiscale modeling of radiation damage in Fe-based alloys in the fusion environment

B.D. Wirth [a,*], G.R. Odette [b], J. Marian [c], L. Ventelon [a], J.A. Young-Vandersall [d], L.A. Zepeda-Ruiz [d]

[a] Department of Nuclear Engineering, University of California, Berkeley, CA 94720-1730, USA
[b] Department of Mechanical and Environmental Engineering, University of California, Santa Barbara, CA 93106, USA
[c] Graduate Aeronautical Laboratories, California Institute of Technology, Pasadena, CA 91125, USA
[d] Lawrence Livermore National Laboratory, P.O. Box 808, Livermore, CA 94551, USA

**Abstract**

Ferritic alloys represent a technologically important class of candidate materials for fusion first wall and blanket structures. A detailed understanding of the mechanisms of defect accumulation and microstructure evolution, and the corresponding effects on mechanical properties is required to predict their in-service structural performance limits. The physical processes involved in radiation damage, and its effects on mechanical properties, are inherently multiscale and hierarchical, spanning length and time scales from the atomic nucleus to meters and picosecond to decades. In this paper, we present a multiscale modeling methodology to describe radiation effects within the fusion energy environment. Selected results from atomic scale investigation are presented, focusing on (i) the mechanisms of self-interstitial dislocation loop formation with Burgers vector of $a\langle 1\,0\,0\rangle$ in iron relative to vanadium, (ii) helium transport and (iii) the interaction between helium and small self-interstitial clusters in iron, and (iv) dislocation-helium bubble interactions in fcc aluminum.


## 1. Introduction

Fusion power plant first wall and blanket systems arguably represent the single greatest structural materials challenge of all time. Even moderate performance goals will place totally unprecedented and unexplored demands on materials and structures. Exposure to high-energy radiation severely damages the microstructure of materials by violently displacing atoms from their lattice sites many times and creating damaging concentrations of helium and hydrogen. The resulting microstructural and damage evolutions cause profound macroscopic property changes that severely degrade the performance and lifetime limits of first wall components [1–4].

The effect of irradiation on materials microstructure and properties is a classic example of an inherently multiscale phenomenon. Pertinent processes range from the atomic nucleus to structural component length scales, spanning in excess of 10 orders of magnitude, while time scales bridge more than 22 orders of magnitude [5]. Further, a wide range of variables controls the mix of nano/microstructural features formed, and the corresponding degradation of physical and mechanical properties. The most important variables include the initial material microstructure, the thermal mechanical loads and irradiation history. Yet, radiation damage is the overarching concern for first wall and breeding blanket structures [2].

At the smallest scales, radiation damage is continually initiated with the formation of energetic primary

* Corresponding author. Tel.: +1-510 642 5341; fax: +1-510 643 9685.
*E-mail address:* bdwirth@nuc.berkeley.edu (B.D. Wirth).

0022-3115/$ - see front matter © 2004 Elsevier B.V. All rights reserved.
doi:10.1016/j.jnucmat.2004.04.156

knock-on atoms through collisions between high-energy neutrons and lattice atoms. Concurrently, high concentrations of insoluble helium and hydrogen gas are generated in (n,$\alpha$) and (n,p) neutron capture reactions, which have threshold energies above several MeV, hence are not normally produced in high quantities in fission neutron irradiations [6]. The primary knock-on atoms, as well as recoiling transmutant nuclei quickly lose kinetic energy through a chain of atomic collision displacements, generating a displacement cascade of vacancy and self-interstitial defects, in addition to electronic excitations. High-energy displacement cascades evolve over very short times, 100 picoseconds or less, and small volumes, with characteristic length scales of 50 nm or less, and are directly amenable to molecular dynamics (MD) simulations [7–9]. The physics of primary damage production in high-energy displacement cascades has been extensively studied with MD simulations and described in a number of excellent review articles [7–9]. The key conclusions from cascade studies are that (i) intra-cascade recombination of vacancies and self-interstitial atoms (SIAs) results in $\sim$30% of the defect production expected from simple primary displacement theory, (ii) many-body collision effects produce a spatial correlation (separation) of the vacancy and SIA defects, (iii) substantial clustering of the SIAs and to a lesser extent, the vacancies occurs within the cascade volume, and (iv) high-energy displacement cascades tend to break up into lobes, or sub-cascades which may also enhance recombination [8,9].

Nevertheless, it is the diffusional transport and evolution of the defects produced in displacement cascades, in addition to solutes and transmutant impurities, that ultimately dictates radiation damage accumulation and changes in materials microstructure at nanometer/micrometer length scales. The evolution of local chemistry and structure at these scales is responsible for changes in physical and mechanical properties [10–12]. Spatial and temporal correlations associated with the displacement cascades continue to play an important role over much larger scales, as do processes including defect recombination, clustering, migration, and gas and solute diffusion and trapping. Over such length and time scales, it is the time and temperature kinetics of diffusive and reactive processes, both within (cascade aging) and outside (long range migration) that govern micro/nanostructural evolution, albeit strongly influenced by the underlying sink structure of the microstructure and the continual production of new radiation damage.

While many of the controlling radiation damage processes and kinetics are known, quantitative details regarding the interactions amongst evolving species and indeed, even the transport, trapping/de-trapping and annihilation mechanisms of small defect-impurity clusters remain to be established. Fortunately, recent innovations in computational modeling, coupled with increasingly powerful high-performance computing and improved experimental tools, provide a basis to develop validated multiscale models of fusion materials performance. However, it is important to note that the complexity of modern engineering materials and multiple degradation processes occurring in the severe fusion environment makes this a tremendous long-term challenge, certainly on par with simulating a burning fusion plasma.

The next section describes a hierarchical multiscale modeling approach to simulating fusion materials performance. The remainder of the paper presents selected results from atomic scale investigations of defect transport and evolution, namely (i) the mechanisms governing the formation of self-interstitial dislocation loops with Burgers vector of $a\langle 1\,0\,0\rangle$ in ferritic relative to vanadium alloys, (ii) the atomistic mechanisms of He transport and (iii) the interaction of helium with small SIA clusters in iron. Finally, before summarizing the article, we address the use of atomistic simulations to provide insight into radiation hardening by describing the interaction between moving edge dislocations with helium bubbles in fcc aluminum.

## 2. Multiscale modeling approach

Fig. 1 provides a schematic view of a multiscale modeling approach that integrates experimental and computational techniques to investigate materials degradation in the fusion environment. This approach is hierarchical and based on passing information or parameters, and connecting key mechanisms, starting from the electronic/atomic up to structural length and time scales. Fig. 1 illustrates a range of simulation and experimental techniques used throughout both the US and international fusion materials research programs, although the focus of this particular paper is on atomic-scale modeling.

The modeling methodology illustrated in Fig. 1 includes ab initio electronic structure calculations, molecular dynamics (MD), kinetic Monte Carlo (KMC), field equations or rate theory simulations with thermodynamics and kinetics by passing information about the controlling physical mechanisms between modeling techniques over the relevant length and time scales. The key objective of such an approach is to track the fate of solutes, impurities and defects during irradiation and thereby, to predict microstructural evolution. Detailed microstructural information serves as a basis for modeling the mechanical behavior through meso (represented by kinetic Monte Carlo and 3D dislocation dynamics) and continuum scale models, which must be incorporated into deformation and fracture mechanics models at the continuum finite element modeling scale to predict failure limits on both the test coupon and com-

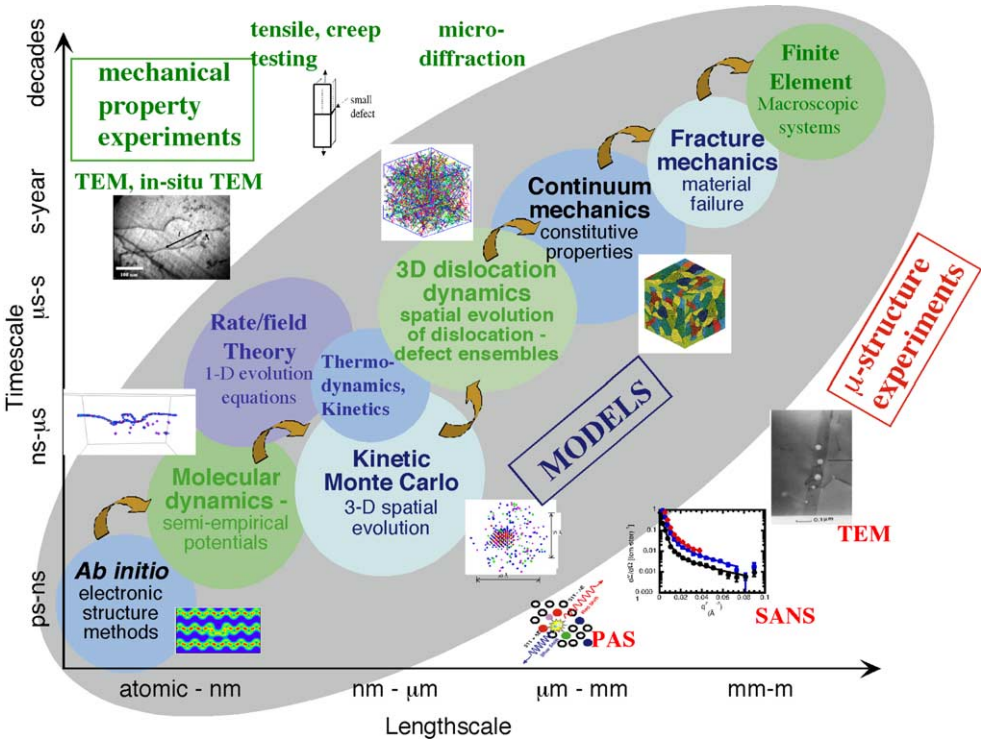


Fig. 1. Illustration of an integrated experimental and computational approach to the multiscale investigation of materials behavior in the fusion environment. The central part of the figure describes an hierarchical approach based on passing information or parameters, and connecting key mechanisms (denoted by arrows), starting from the electronic/atomic up to structural length and time scales. A number of microstructural characterization techniques important for validating model predictions are represented on the lower right side, including the techniques of positron annihilation spectroscopy (PAS), small angle neutron scattering (SANS) and transmission electron microscopy (TEM). The upper left side of the diagram represents experimental techniques to measure mechanical properties.

ponent scale [13]. In this figure, individual modeling techniques are identified within a series of linked process circles, which also shows the overlap of relevant length and timescales. The passing of information between the scales is represented through a series of arrows. While not explicitly discussed in this paper, the availability and accuracy of interatomic potentials, including those for multicomponent alloys, represent a major issue in multiscale modeling, especially in the use of atomistic modeling techniques like MD and KMC. The impact of potential uncertainties varies with the modeling task, but emphasizes the importance of comparing results amongst modeling techniques and experiments for self-consistency and validation.

Of course, multiscale modeling by itself is insufficient to fully predict the performance of complicated engineered structures in the fusion environment, and a science-based multiscale paradigm necessitates a close integration between experiments and modeling. Fig. 1 also illustrates a select set of experimental techniques commonly used in fusion materials research to characterize microstructures and determine mechanical properties. The lower right side of the figure represents the microstructural characterization techniques of small angle scattering, positron annihilation and transmission electron microscopy (TEM). The upper left side of the figure represents techniques commonly used for evaluating the mechanical behavior of irradiated engineering materials, including tensile and creep testing, and dislocation structure characterization by TEM and microdiffraction techniques. Of particular importance for comparing experiment and simulation results is the increasing application of in-situ studies [14].

## 3. Self-interstitial dislocation loops in Fe and V alloys

It is well established that TEM examination of ferritic alloys following low dose, intermediate temperature irradiation (<0.05 displacement per atom, dpa, at 300 °C) by neutrons or heavy ions does not reveal any visible damage. However, as the irradiation dose increases above ~0.05 dpa, a significant population of dislocation loops, primarily of interstitial type, is experimentally observed with $\mathbf{b} = a\langle 1\,0\,0\rangle$ and $\mathbf{b} = a/2\langle 1\,1\,1\rangle$. The distribution of loop Burger's vectors observed ranges from

almost equal proportions to predominantly $a\langle 1\,0\,0\rangle$ in some cases, rather than the expected and lowest energy $\mathbf{b} = a/2\langle 1\,1\,1\rangle$. While this result has been known for nearly 40 years [15–17], the mechanisms responsible for the presence of $\langle 1\,0\,0\rangle$ loops in ferritic alloys has not been established until recently [18].

In contrast to ferritic alloys, fewer studies have been performed to characterize the Burger's vector of dislocation loops formed in irradiated vanadium alloys, and the resulting microstructural trends are less clear. Different research groups have reported loops with one or more of the following Burger's vectors, $a/2\langle 1\,1\,1\rangle$, $a\langle 1\,0\,0\rangle$ and even those of $a/2\langle 1\,1\,0\rangle$ faulted loops. Rice and Zinkle observe that following neutron irradiation in a V–4Cr–4Ti alloy, the dislocation loops are $a/2\langle 1\,1\,0\rangle$ type at low temperature, but transition to $a/2\langle 1\,1\,1\rangle$ at high temperature [19]. Other observations indicate that the loops are all of $a/2\langle 1\,1\,1\rangle$ type [20]. Matsui and coworkers observe both perfect loop types, with about 50% $a\langle 1\,0\,0\rangle$ and 50% $a/2\langle 1\,1\,1\rangle$ in pure vanadium, and varying mixtures of $a\langle 1\,0\,0\rangle$ and $a/2\langle 1\,1\,1\rangle$ Burger's vectors in vanadium alloys, depending on the atomic size of alloying elements [21].

A mechanism to explain the formation and growth of $\langle 1\,0\,0\rangle$ loops in α-Fe has recently been proposed [18] and will be briefly summarized here within the context of comparing vanadium to iron. Experiments performed in Fe and Mo in the early 1960's showed the formation of hexagonal dislocation networks composed of $\frac{1}{2}\langle 1\,1\,1\rangle$ and $\langle 1\,0\,0\rangle$ dislocation segments. The $\langle 1\,0\,0\rangle$ segments were presumed to form as a result of interactions, according to the reaction [15,18]:

$$\frac{1}{2}[1\,1\,1] + \frac{1}{2}[1\,\bar{1}\,\bar{1}] \rightarrow [1\,0\,0]. \tag{1}$$

In 1965, Masters recognized that the reaction in Eq. (1) could rationalize the observation of $\langle 1\,0\,0\rangle$ loops in thin-film ion irradiation studies [15]; however, he discounted this possibility since $\frac{1}{2}\langle 1\,1\,1\rangle$ loops were not observed in his studies. Yet, it is now recognized that not only are such loops directly produced in displacement cascades, but that they also exhibit a very high mobility for one-dimensional motion defined by the $\langle 1\,1\,1\rangle$ glide cylinder [8,9].

Fig. 2 presents the results of MD simulations, performed using Finnis–Sinclair $N$-body potentials, to determine the self-energy of $a/2\langle 1\,1\,1\rangle$ and $a\langle 1\,0\,0\rangle$ SIA dislocation loops in α-Fe and V. As expected from continuum elasticity theory, the loops with $a\langle 1\,0\,0\rangle$ have a higher self-energy than $\frac{1}{2}\langle 1\,1\,1\rangle$ in both cases. However, the difference in energy is much smaller in α-Fe than expected, raising the possibility of the formation and existence of metastable $a\langle 1\,0\,0\rangle$ loops.

MD simulations of interactions (collisions) between SIA dislocation loops reveal that junctions of $a\langle 1\,0\,0\rangle$ type do form in both V and α-Fe consistent with Eq. (1). The necessary conditions for $\langle 1\,0\,0\rangle$ junction formation for the reactor described in Eq. (1) are that both interacting clusters are approximately the same size, are larger than ~20 SIAs, and, possibly, have the same shape [18]. When these conditions are not met, the smaller cluster always rotates into the $\langle 1\,1\,1\rangle$ orientation of the larger cluster in both iron and vanadium [18,22].

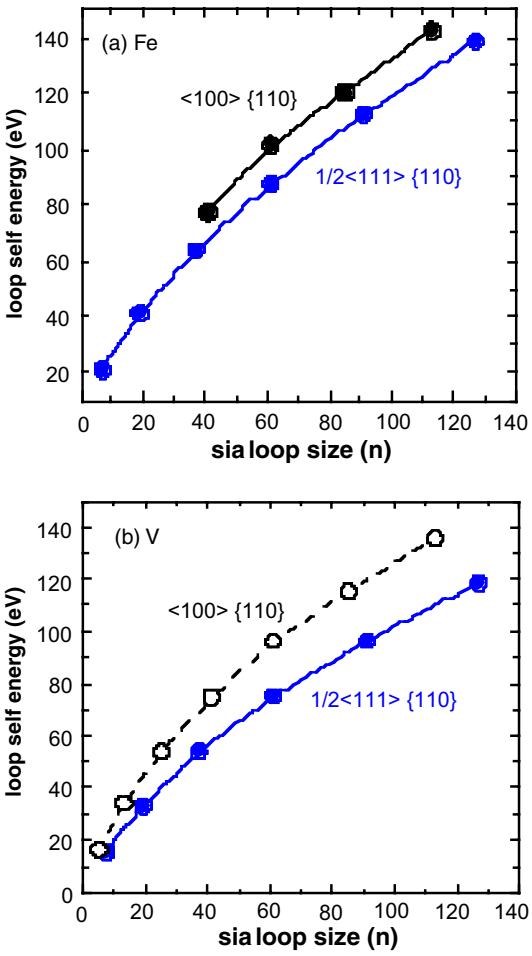


Fig. 2. Self-energy of self-interstitial atom dislocation loops of Burgers vector $a/2\langle 1\,1\,1\rangle$ (blue) and $a\langle 1\,0\,0\rangle$ (black) in (a) iron and (b) vanadium. The data points are computer simulation results and the line is a fit to the continuum elasticity energy expression.

While $\langle 1\,0\,0\rangle$ junctions are predicted to form in both vanadium and iron, the junction stability is very different in the two cases, and we believe this may control the differences in observed dislocation loop populations. In vanadium, the junctions are thermally unstable and the final configuration observed in MD simulations at temperatures between 400 and 700 K is a single $\frac{1}{2}\langle 1\,1\,1\rangle$ loop. In contrast, the junction in iron is thermally (meta-) stable and can propagate across the loop through a

complicated two-step mechanism described by Marian and co-workers [18].

The conclusion from these computer simulations is that $a\langle 1\,0\,0\rangle$ loops can form and grow in iron, likely in conjunction with a population of interacting $a/2\langle 1\,1\,1\rangle$ loops [18,23]. However, in vanadium, the $a/2\langle 1\,1\,1\rangle$ loops predominate, due to the instability of the $a\langle 1\,0\,0\rangle$ junctions. It is possible that the underlying cause of the different junction stability is related to corresponding differences of the single self-interstitial atom [24], although that remains to be determined.

## 4. Atomistics of He diffusion

One of the key challenges facing the development of high performance, long-lived fusion materials is managing the high level of helium generated in first wall and blanket structures. It is believed that helium from (n,α) reactions initially resides in interstitial sites and is very mobile. MD studies recently performed by Morishita and co-workers, with improved interatomic potentials, have determined an activation energy of 0.08 eV for interstitial He migration in α-Fe [25]. However, helium is deeply trapped in vacancies, and then behaves similar to a substitutional solute [26]. A helium–vacancy binding energy of 3.7 eV has been determined from these same MD simulations [25]. Strong binding of helium atoms with dislocations and grain boundaries has also been calculated by other groups with the same potentials [27]. Thus diffusion of substitutional helium (trapped at a vacancy), occurs via a vacancy mechanism. We have used these same set of potentials in MD simulations to investigate the properties and diffusion of substitutional helium, within the framework of the multiple jump frequency analysis proposed by Le Claire [28].

Notably, substitutional helium interacts more strongly with neighboring vacancies than, for example, a typical oversized solute like copper, with binding energies of 0.46 and 0.19 eV with first and second nearest neighbor vacancies, respectively. He exchanges rapidly between the two neighboring vacant sites in a nearly $\langle 1\,1\,1\rangle$ trajectory at a frequency $\omega_2$. The position of the helium atom within the di-vacancy is delocalized, with a preferred symmetrical location in lattice units of (0.11, 0.11, 0.11) or (0.39, 0.39, 0.39), rather than the vacant lattice sites at (0, 0, 0) and (0.5, 0.5, 0.5). The saddle point activation energy for exchanges between the two preferred locations is just 0.015 eV.

Hence, the diffusion of helium in the bcc crystal structure is governed by the jumps of vacancies to and from neighboring lattice sites, and not the direct nearest neighbor exchange [28]. The most important jumps are from the first nearest to the third nearest and second nearest neighbor positions, respectively at frequencies of $\omega_3'$ and $\omega_3$. Fig. 3 shows the energy barriers for $\omega_3'$ and $\omega_3$ vacancy–Fe lattice atom exchanges calculated by molecular statics (MS), with activation energies of 1.1 and 1.13 eV, respectively. As a reference, the MS calculations give a value of 0.85 eV for the activation energy of an iron atom jumping into a nearest neighbor vacancy in a pure Fe lattice, which also occurs along a $\langle 1\,1\,1\rangle$ trajectory. The solute impurity diffusion is calculated in the Le Claire model as:

$$D_{\mathrm{He}} = d^2 f_{\mathrm{He}} \omega_2 \exp\left(\frac{S^{\mathrm{v,f}}}{k}\right) \exp\left(-\frac{(E^{\mathrm{v,f}} - E^{\mathrm{b,He-v}})}{kT}\right), \tag{2a}$$

where $f_{\mathrm{He}}$ is the correlation factor for He diffusion given by

$$f_{\mathrm{He}} = \frac{u}{\omega_2 + u}, \tag{2b}$$

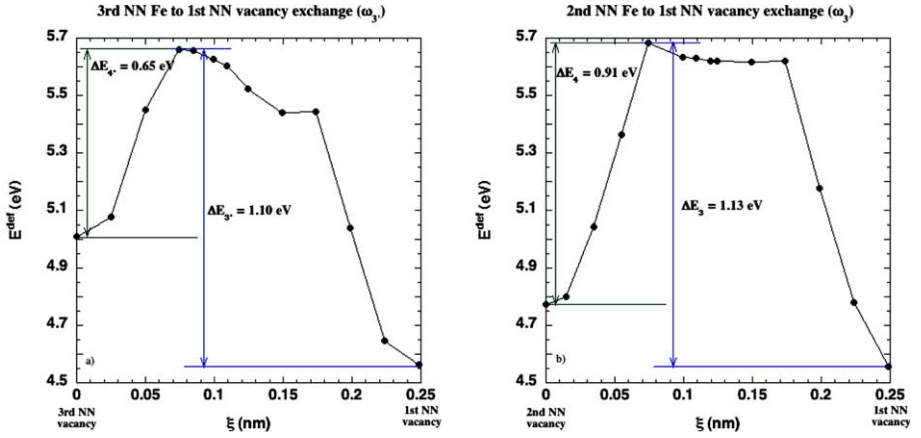


Fig. 3. Calculated activation energies for iron–vacancy exchanges of (a) 3rd to 1st nearest neighbor and (b) 2nd to 1st nearest neighbor in the vicinity of a substitutional He atom.

$$u = \frac{1}{2}\omega_{3'}\left(3 + 2\beta + \frac{0.51\beta}{0.51+\beta}\right). \quad (2c)$$

In these equations, $d$ is the nearest neighbor spacing ($\sqrt{3}/2 \times 0.287$ nm), $G^{v,f}$ is the free energy of isolated vacancy formation $= E^{v,f}$ (1.71 eV) $- TS^{v,f}$ ($\sim$1–1.5 k), $E^{b,He-v}$ is the first nearest neighbor vacancy–helium binding (0.46 eV) and $\beta_3 = \omega_3/\omega_{3'}$. Assuming that $\omega_i = v_o \exp(S^{v,m}/k)\exp(-\Delta E_i/kT)$ with $v_o = 10^{13}$ s$^{-1}$ and $S^{v,m} \sim$ 1–1.5 k, $S(= S^{v,f} + S^{v,m}) \sim 2$–$3k$, and $\exp(S/k) \approx 10$ [29], yields $D_{He} = 1.6 \times 10^{-5} \exp(-2.35/\mathrm{kT})$ m$^2$/s.

The effective activation energy of 2.35 eV for thermal helium diffusion can be understood as follows. The activation energy for helium–nearest neighbor vacancy exchange is very low ($\Delta E_2 = 0.015$ eV), thus $\omega_2 \gg u$ and $f_{He} \approx u/\omega_2$. Similar jump frequencies for first to third and first to second nearest neighbor positions ($\omega_{3'}$ and $\omega_3$, respectively), the definition of $\beta$ and its average value of $0.5 \pm 0.2$ over the temperature range of 200–1000 °C, give $u \approx 2.1\omega_3$, and thus, $f_{He} \sim 2.1\omega_{3'}/\omega_2$. This leads to the following approximation for thermal helium diffusion

$$D_{He} \approx 2.1 d^2 v_O \exp\left(\frac{S}{k}\right)\exp\left(-\frac{(E^{v,f} + \Delta E_{3'} - E^{b,He-v})}{kT}\right) \quad (3)$$

which gives a pre-factor of $1.3\times10^{-5}$ m$^2$/s and an activation energy of 2.35 eV ($= 1.71 + 1.1 - 0.46$ eV), close to the full numerical solution. Notably, neither the temperature effects or the quantitative values associated with the vacancy formation and migration entropy, nor magnetic effects below the Curie temperature, are included in Eqs. (2) and (3), but these factors will be assessed in the future.

Additionally, our MS calculations have shown that substitutional helium can directly exchange with a second nearest neighbor vacancy, along a trajectory close to $\langle 1\,0\,0\rangle$, with an activation energy of 0.66 eV [30]. Similar behavior was observed in earlier computational studies of helium diffusion in molybdenum [31]. However, solute atom exchanges with second nearest neighbor vacancies are not currently included in Le Claire's model [28]. The implications of direct second nearest neighbor exchanges to helium diffusion are currently being assessed by Monte Carlo methods and will be reported in a future publication.

## 5. He–SIA interactions in α-Fe

We have performed MD simulations of the interactions of helium with both SIA and SIA clusters. An example is given in Fig. 4, which shows MD snapshots of the interaction between an individual self-interstitial atom in Fe and two neighboring helium substitutional atoms at 600 K. Initially, the SIA is 1.3 nm away from the He atom that is furthest to the right. Over several picoseconds, the SIA migrates three-dimensionally, with multiple changes of direction (orientation), towards the nearest helium atom and by Fig. 4(b), is about 0.6 nm away. This is followed by a rapid and spontaneous recombination-replacement reaction as the SIA enters the vacant lattice site, thereby ejecting the helium atom from a substitutional to an interstitial position. Of course, it is known a priori that the reaction is energetically favorable, since the SIA–vacancy Frenkel pair formation energy of about 6.5 eV is larger than the interstitial helium energy of 5.25 eV. The simulation reveals a long-range interaction between the SIA and substitutional helium; however the effective recombination-replacement radius remains to be quantified. The ejected interstitial helium subsequently diffused rapidly until it encountered the nearby substitutional helium, forming a trapped complex that did not migrate over an additional 40 ps at 600 K. The strong interstitial helium trapping at the He2Vl complex is notable, although the dissociation and migration mechanisms and energies of such complexes remain to be determined.

MD simulations have also been performed between 400 and 1000 K to determine the interaction between substitutional He atoms and one-dimensionally migrating SIA clusters containing between $m = 6$ and 20 SIAs. The results indicate a wide range of possible interactions, including SIA/V recombination and He recombination-replacement reaction producing a strongly bound $m - 1$ SIA–He cluster complex that is immobile over MD times of order 100 ps, the normative time associated with rapid $\langle 1\,1\,1\rangle$ migration of pure SIA clusters. SIA–He cluster complex formation was observed for both interstitial and substitutional helium, although the interactions are stronger in the former case. MS calculations of 6 SIA–interstitial He cluster complex reveal a binding energy of 1.5 eV, which indicates that such a complex would be strongly trapped even up to high temperature.

Many open questions remain regarding the interaction between SIA and SIA clusters and helium, including site-dependent manifolds of trapping/binding energies as a function of cluster size and the mobility and migration mechanisms of SIA–He clusters. The results presented here are an initial step towards cataloging and quantifying a wide range of mechanisms and parameters that are needed in microstructural evolution models. Key phenomena are currently being modeled, including the interaction between SIA loops and helium bubbles along with helium trapping, migration and clustering reactions at precipitate interfaces, dislocations and grain boundaries, and will be reported in the future.

## 6. Dislocation – He bubble interactions

Following irradiation at low to intermediate temperatures, metallic materials exhibit an increase in yield

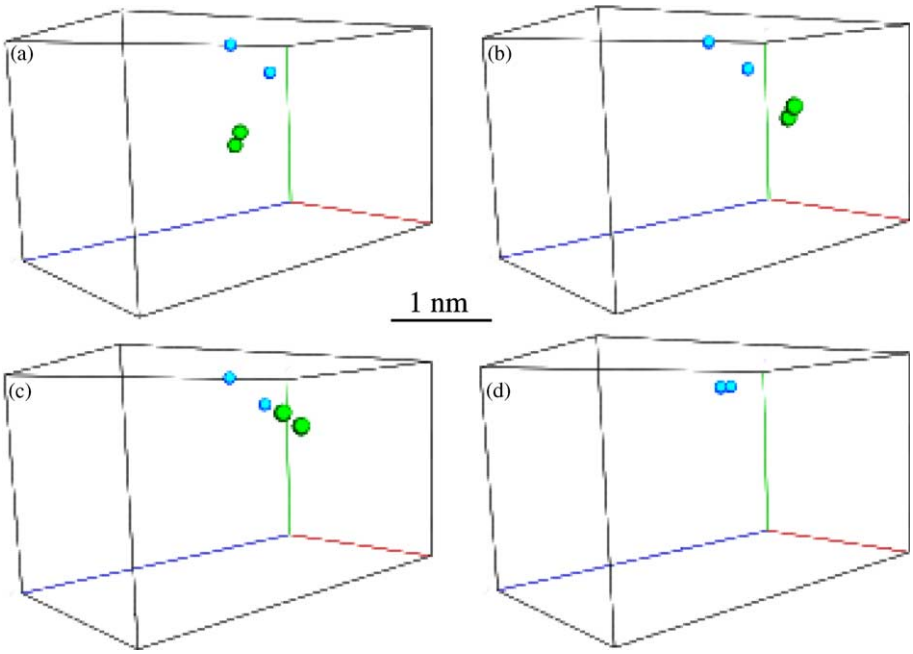


Fig. 4. MD simulations showing the interaction between a self-interstitial atom (two green circles) with two substitutional helium atoms (light blue circles) in iron at 600 K. The SIA migrates towards the nearest helium atom, where it recombines with the vacancy, ejecting the helium to an interstitial position. The interstitial helium atom migrates three-dimensionally until it encounters and traps at the other substitutional helium atom in a $He_2V_1$ complex.

and ultimate strength, along with a decrease in uniform and total failure strains and strain hardening rate [32–34]. Irradiation hardening is primarily due to the formation of fine scale microstructural features that act as obstacles to dislocation slip. While bubbles are observed in materials at sufficiently high helium concentrations that depend on the irradiation temperature, their role in hardening remains to be resolved.

MD simulations are an ideal tool to investigate such deformation phenomena since they directly account for dislocation core and non-linear effects not treated within elastic theory and provide atomistic information regarding the mechanisms and sequence-of-events in dislocation–obstacle interactions. As an illustration of the power of MD simulations, we present an example of the interaction between an edge dislocation and an under-pressurized, 2.6 nm diameter helium bubble. Further details regarding the use of MD for simulating dislocation–obstacles interactions are published elsewhere [35–38].

Fig. 5 shows MD simulations of the interaction in Al between a dissociated edge dislocation, separated into two Shockley partial dislocations, and an under-pressurized He bubble in Al. The dislocation bypass mechanism involves the successive shearing of the bubble by one Burger's vector with each passage of a dislocation. At the atomic scale, each partial dislocation segment locally annihilates at the leading surface of the bubble

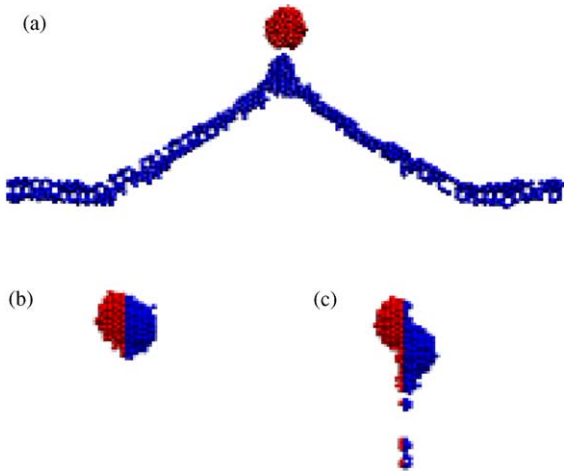


Fig. 5. MD simulation snapshots of the interaction between an edge dislocation and a 1.3 nm radius helium bubble in aluminum with an applied shear stress of 100 MPa at 100 K. (a) The configuration of the dislocation core (blue circles) as it bypasses the helium bubble (red circles) the first time. Edge on perspectives of the He bubble are shown following the passage of (b) two and (c) six dislocations. Red and blue circles denote atoms below and above the dislocation glide plane, respectively. Note that successive dislocation interactions remove some helium from the bubble.

and re-nucleates on the trailing surface as it breaks away from the obstacle. Although not observed in these simulations, over longer times the high surface diffusivity at the solid–vapor interface can heal the sheared bubble.

In addition to revealing the interaction mechanism, it is important to characterize the obstacle strength. Unfortunately, intrinsically high strain rate MD simulations generally underestimate the critical bypass angle and thus over estimate the obstacle strength [37]. To more accurately determine the critical stress, a series of MD simulations were performed in which the applied shear stress was decreased from 100 MPa to determine the stress needed to bypass the periodic array of 2.6 nm diameter cavities, with a range of helium pressures, and an obstacle spacing of 30 nm. For a void containing no helium, the critical stress in the MD simulations is ≈25 MPa, which corresponds to an obstacle strength, $\alpha = 0.1$ by comparing to the expression

$$\tau_{\mathrm{crss}} = \frac{0.8\alpha G b}{\Lambda}, \tag{4}$$

where $\Lambda$ is the obstacle spacing, $b$ is the Burger's vector and $G$ is the shear modulus. The introduction of helium into the cavity at a He/vacancy ratio = 0.5 (e.g. an internal pressure of 90 MPa) produces a slightly larger critical stress of 35 MPa, and corresponds to a stronger obstacle, with $\alpha = 0.14$. Future simulations will quantify the effect of He pressure on the critical stress, as well as the effect of image interactions from the periodic array of dislocations.

## 7. Conclusion

We have outlined a multiscale approach to modeling radiation damage. The approach, like radiation damage and its consequences themselves, is inherently hierarchical and is based on passing information on parameters and controlling mechanisms up from the electronic or atomic scales to micro-, meso, continuum and structural length and time scales. The paper illustrates the approach with select results from atomic scale investigations of the behavior and interaction between SIA clusters/dislocation loops, helium, helium bubbles and dislocations in iron, vanadium and aluminum using Finnis–Sinclair and embedded atom method potentials for the metal–metal interactions and pair potentials fit to quantum mechanical computations to describe the metal–helium interactions. The results illustrate a range of phenomena occurring during irradiation in the fusion environment that require further investigation and incorporation into comprehensive microstructural evolution and property change models.

1. MS simulations in iron and vanadium show that $a/2\langle 1\,1\,1\rangle$ dislocation loops are the lowest energy configuration for SIA clusters. However, in iron $a\langle 1\,0\,0\rangle$ loops are closer in energy to the $a/2\langle 1\,1\,1\rangle$ loops than is predicted by dislocation elasticity theory, indicating the possibility of metastable $a\langle 1\,0\,0\rangle$ loops. The corresponding energy differences are larger in the case of vanadium.
2. Reactions between $a/2\langle 1\,1\,1\rangle$ loops can in certain circumstances form $a\langle 1\,0\,0\rangle$ junctions in both vanadium and iron. In vanadium, the junctions are thermally unstable and rapidly dissolve as the loops rotate to form a single $a/2\langle 1\,1\,1\rangle$ dislocation loop. In iron, the junction is stable over an intermediate temperature regime and can propagate, to form a $a\langle 1\,0\,0\rangle$ dislocation loop.
3. Atomistic simulations in iron within the framework of the multiple frequency diffusion model of Le Claire [28] indicate a thermal diffusion activation energy of 2.35 eV for substitutional helium. The simulations reveal that helium is strongly delocalized in a di-vacancy–helium complex and that substitutional helium can exchange with a second nearest neighbor vacancy with an activation energy of 0.66 eV.
4. MD simulations in iron of the interactions between substitutional helium and SIA, reveal strong interactions leading to SIA–V recombination and replacement reactions that spontaneously eject helium into an interstitial site. The simulations indicate strong helium trapping and short time immobility of SIA–He cluster complexes. For example, the calculated binding energy of a 6-SIA – interstitial helium cluster complex is 1.5 eV.
5. MD simulations in aluminum of the interaction between an edge dislocation and a periodic array of under-pressurized He bubbles with a mean spacing of 30 nm, reveals a critical shear stress of 35 MPa and thus, an obstacle strength, $\alpha = 0.14$. The dislocation bypass mechanism involves the local annihilation and re-nucleation of partial dislocation segments, producing a shear step in the bubble.

## Acknowledgements

This work has been partially supported by the Office of Fusion Energy Sciences, US Department of Energy under Grant DE-FG02-04ER54750 at UCB and Grant DE-FG02-04ER54275 at UCSB, and partially performed under the auspices of the US Department of Energy and Lawrence Livermore National Laboratory under contract W-7405-Eng-48.

## References

[1] E.E. Bloom, J. Nucl. Mater. 258–263 (1998) 7.
[2] E.E. Bloom, N. Ghoniem, R. Jone, R. Kurtz, G.R. Odette, A. Rowecliffe, D. Smith, F.W. Wiffen, Advanced Materials

Program, appendix D of the VLT roadmap, 1999. Available from http://vlt.ucsd.edu/.
[3] S.J. Zinkle, N.M. Ghoniem, Fus. Eng. Des. 51&52 (2000) 55.
[4] T. Muroga, M. Gasparotto, S.J. Zinkle, Fus. Eng. Des. 61&62 (2002) 13.
[5] G.R. Odette, B.D. Wirth, D.J. Bacon, N.M. Ghoneim, MRS Bull. 26 (2001) 176.
[6] R.E. Stoller, G.R. Odette, H.L. Heinisch, A whitepaper proposing an integrated program of theoretical, experimental and database research for the development of advanced fusion materials, prepared for the Office of Fusion Energy Sciences, US Department of Energy, 1999.
[7] J.B. Gibson, A.N. Goland, M. Milgram, G.H. Vineyard, Phys. Rev. 120 (1960) 1229.
[8] A.F. Calder, D.J. Bacon, J. Nucl. Mater. 207 (1993) 25.
[9] W.J. Phythian, R.E. Stoller, A.J.E. Foreman, A.F. Calder, D.J. Bacon, J. Nucl. Mater. 223 (1995) 245.
[10] G.R. Odette, J. Nucl. Mater. 85&86 (1979) 533.
[11] L.K. Mansur, E.E. Bloom, J. Met. 34 (1982) 23.
[12] B.N. Singh, A.J.E. Foreman, J. Nucl. Mater. 122&123 (1984) 537.
[13] G.R. Odette, T. Yamamoto, H.J. Rathbun, M.Y. He, M.L. Hribernik, J.W. Rensman, J. Nucl. Mater. 323 (2003) 313.
[14] J.S. Robach, I.M. Robertson, B.D. Wirth, A. Arsenlis, Philos. Mag. A 83 (2003) 955.
[15] B.C. Masters, Philos. Mag. 11 (1965) 881.
[16] B.L. Eyre, A.F. Bartlett, Philos. Mag. 11 (1965) 261.
[17] A.C. Nicol, M.L. Jenkins, M.A. Kirk, Mater. Res. Soc. Symp. 650 (2001) R1.3.
[18] J. Marian, B.D. Wirth, J.M. Perlado, Phys. Rev. Lett. 88 (2002) 255507.
[19] P.M. Rice, S.J. Zinkle, J. Nucl. Mater. 258–263 (1998) 1414.
[20] D.S. Gelles, P.M. Rice, S.J. Zinkle, H.M. Chung, J. Nucl. Mater. 258–263 (1998) 1380.
[21] H. Matsui, H. Nakajima, S. Yoshida, J. Nucl. Mater. 205 (1993) 452.
[22] Y.N. Osetsky, A. Serra, V. Priego, J. Nucl. Mater. 276 (2000) 202.
[23] J. Marian, B.D. Wirth, R. Schaublin, G.R. Odette, J.M. Perlado, J. Nucl. Mater. 323 (2003) 181.
[24] L.A. Zepeda-Ruiz, J. Marian, B.D. Wirth, Philos. Mag., submitted for publication.
[25] K. Morishita, B.D. Wirth, T. Diaz de la Rubia, A. Kimura, in: S. Hanada, Z. Zhong, S.W. Nam, R.N. Wright (Eds.), Proceedings of the 'The Fourth Pacific Rim International Conference on Advanced Materials and Processing (PRICM4)', The Japan Institute of Metals, 2001, p. 1383.
[26] W.D. Wilson, R.D. Johnson, in: P.C. Gehlen, J.R. Beeler Jr., R.I. Jaffee (Eds.), Interatomic Potentials and Simulation of Lattice Defects, Plenum, 1972, p. 375.
[27] R.J. Kurtz et al., these Proceedings.
[28] A.D. Le Claire, J. Nucl. Mater. 69&70 (1978) 70.
[29] D.A. Porter, K.E. Easterling, Phase Transformations in Metals and Alloys, Van Nostrand Reinhold, UK, 1981.
[30] B.D. Wirth, E.M. Bringa, Phys. Scr., in press.
[31] R.H.J. Fastenau, L.M. Caspers, A. van Veen, Phys. Status Solidi (a) 34 (1976) 277.
[32] B.N. Singh, A.J.E. Foreman, H. Trinkaus, J. Nucl. Mater. 249 (1997) 103.
[33] A.F. Rowcliffe, S.J. Zinkle, J.F. Stubbins, D.J. Edwards, D.J. Alexander, J. Nucl. Mater. 258–263 (1998) 183.
[34] M. Victoria, N. Baluc, C. Bailat, Y. Dai, M.I. Luppo, R. Schaublin, B.N. Singh, J. Nucl. Mater. 276 (2000) 114.
[35] B.D. Wirth, V. Bulatov, T. Diaz de la Rubia, J. Eng. Mater. Tech. 124 (2002) 329.
[36] J.A. Young, B.D. Wirth, J.S. Robach, I.M. Robertson, J. Nucl. Mater., in preparation.
[37] Y.N. Osetsky, D.J. Bacon, Model. Sim. Mater. Sci. Eng. 11 (2003) 427.
[38] D. Rodney, G. Martin, Phys. Rev. B 61 (2000) 8714.